Supplementary figures

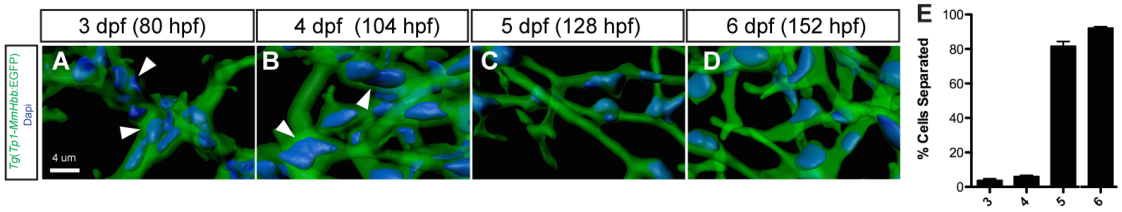

Supplemental figure 1. Biliary epithelial cell remodeling during intrahepatic biliary network formation in zebrafish. (A-D) Projected confocal image of a *Tg(Tp1-MmHbb:*EGFP*)*^{um14} liver visualized for GFP (green) and DAPI (pseudo-color blue) at 3 (A), 4 (B), 5 (C) and 6 (D) dpf. GFP marks the intrahepatic biliary network. Biliary epithelial cells form clusters (white arrowheads) within the intrahepatic biliary network in wild-type larvae at 3 and 4 dpf. However, these cells separate after 5 dpf. **(E)** The percentage of biliary epithelial cells that are not clustered with other biliary epithelial cells.

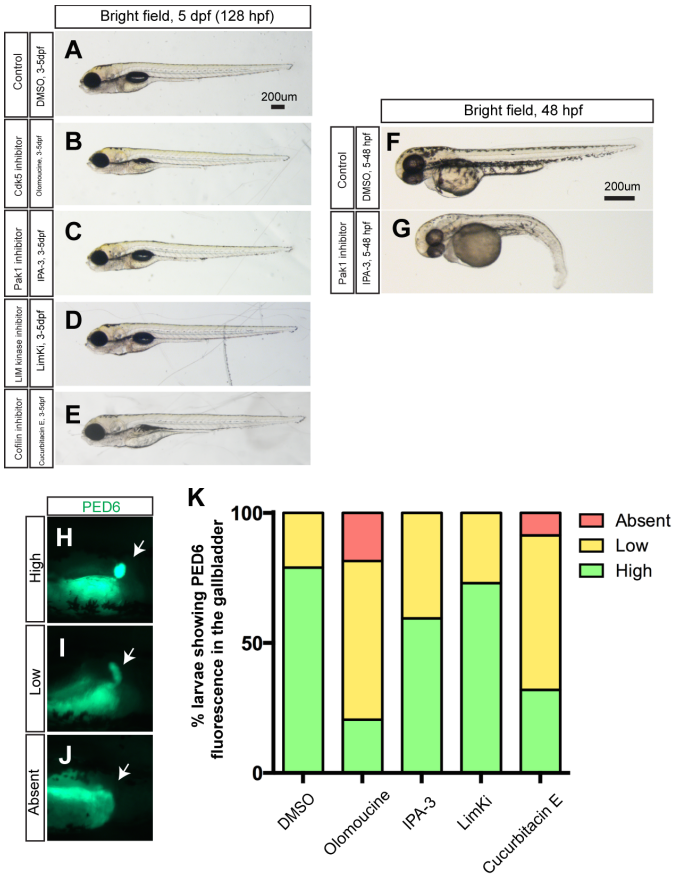

Supplemental figure 2. Larval physical appearance and PED-6 expression in small molecule inhibitor treated larvae. (A-E) Bright field images of control DMSO- (A), olomoucine- (B), IPA-3- (C), LimKi- (D) and cucurbitacin E- (E) treated larvae at 5 dpf. All small molecule inhibitors were treated from 3 to 5 dpf. Lateral views, anterior to the left. These small molecule inhibitors did not induce significant change in larval physical appearance at the concentrations used. Note that none of IPA3-treated larvae (C) showed blood circulation defects (n>50). **(F-G)** The same concentration of IPA-3 (1uM) treatment from 5 to 48 hours induced a phenotype that is indistinguishable from that of Pak1 moprholino injected embryos (Kelly et al., 2014). As seen in Pak1 morpholino injected embryos, these IPA-3-treated embryos did not have blood circulation (n = 9 out of 11). These data suggest that IPA-3 is inhibiting Pak1 function, and Pak1 is dispensable from

proper cardiac morphogenesis after 3 pdf. **(H-J)** Fluorescent images of DMSO- and olomoucine-treated wild-type larvae soaked in PED6. PED6 is processed by phospholipase and fluorescence was detected in the intestine in all treated larvae. However, in some olomoucine-treated larvae, PED6 fluorescence in the gallbladder became weaker (I) or absent (J), compared to strong fluorescence (H) in wild-type larvae. White arrows point to the gallbladder. **(K)** Percentage of larvae showing high, low and no PED6 fluorescence in the gallbladder of DMSO-, olomoucine-, IPA-3-, LimKi- and cucurbitacin E- treated wild-type larvae at 5 dpf.

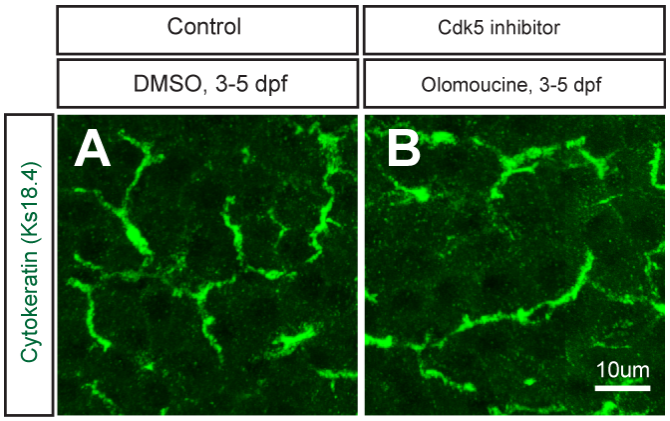

Supplemental figure 3. Cytokeratin staining with DMSO- and olomoucine-treated larvae. (A-B) Projected images of 5 um-thick confocal z-stacks of the liver in DMSO- (A) and olomoucine-treated (B) larvae visualized for Cytokeratin expression at 5 dpf. Cytokeratin is dominantly localized in the intrahepatic biliary network. There was no observable difference in Cytokeratin expression in olomoucine-treated larvae.

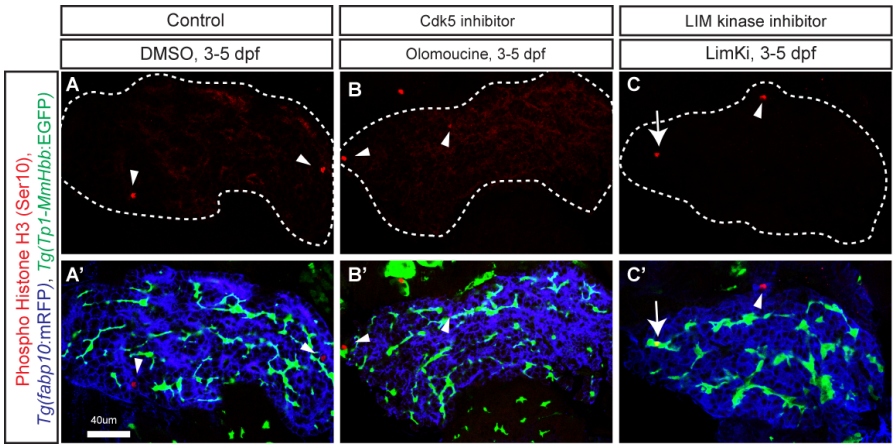

Supplemental figure 4. Cell proliferation measurement in olomoucine- and LIM kinase inhibitor- treated larvae. (A-C) Z-plane confocal images of the liver at 5dpf of DMSO- (A), olomoucine- (B) and LimKi-treated (C) larvae visualized for phospho-Histone H3 (pseudo-colored red) expression. White dotted lines outline the liver. Phospho-Histone H3 expression was merged with *Tg(Tp1-MmHbb:*EGFP)^{um14} (Green) and *Tg(fabp10*:mRFP)^{lri2} (pseudo-colored blue) expression and shown separately in A'-C'. Arrowheads point to Phospho-Histone H3 expression in *Tg(fabp10*:mRFP)^{lri2} positive hepatocytes. Arrow points to Phospho-Histone H3 expression in *Tg(Tp1-MmHbb:*EGFP)^{um14} positive biliary epithelial cells. In the LimKi-treated liver, the number of Phospho-Histone H3 and *Tg(Tp1-MmHbb:*EGFP)^{um14} double positive cells (average 3.75 cells per liver, n=4, SD =0.9, $p<0.05$) increased compared to that of the DMSO-treated liver (average 1.3 cells per liver, n = 4, SD = 1.3), while in the olomoucine-treated liver, the number of double positive cells (average 1.0 cells per liver, n = 5, SD = 0.7) did not change. These data suggest that *Tg(Tp1-MmHbb:*EGFP)^{um14} positive biliary epithelial cells appeared to proliferate more in LimKi-treated larvae.

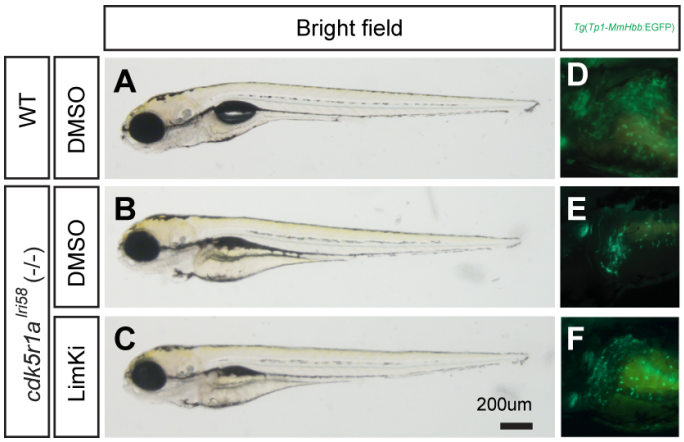

Supplemental figure 5. Larval physical appearance of *cdk5r1a*^{lri58} mutant larvae. (A-C) Bright field images of DMSO-treated wild-type (A) and DMSO- (B) or LimKi-treated (C) *cdk5r1a*^{lri58} mutant larvae at 5 dpf. **(D-F)** Fluorescent image of DMSO-treated wild-type (D) and DMSO- (E) or LimKi-treated (F) *cdk5r1a*^{lri58} mutant *Tg(Tp1-MmHbb:*EGFP*)*^{um14} larvae at 5 dpf.

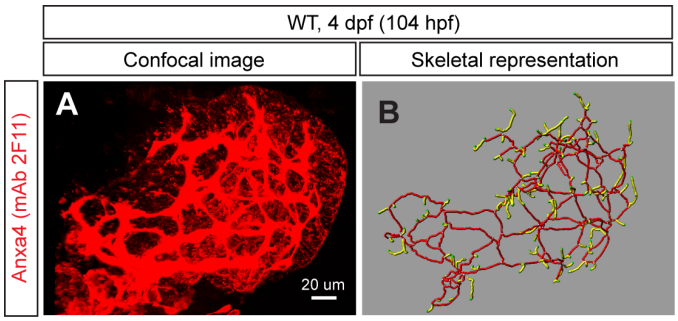

Supplemental figure 6. The skeletal analysis worked with the anti-Anxa4 (mAb 2F11) staining data. (A) Projected confocal image of the wild-type liver visualized for Anxa4 expression by mAb 2F11 staining at 104 hpf. **(B)** Skeletal representations of the intrahepatic biliary network computed based on Anxa4 expression in (A). The liver analysis program developed in this study can analyze the anti-Anxa4 staining data. Ventral views, anterior to the top.

Supplementary Materials and Methods

Design of the Liver Analysis Program 5.3

A custom-developed software written in MatLab 2011b (MathWorks) and packaged as Liver Analysis Program 5.3 was used for all computational skeletal analyses. In the Liver Analysis Program 5.3, in order to segment the GFP positive cells in the cropped region of the confocal z-series, a 3D volume of the biliary network was reconstructed and subsequently fed into a custom-developed connectivity analysis algorithm. The volume was first median filtered to smooth the boundaries of the biliary volume, and then interpolated to an isotropic grid such that the resulting voxel resolution matched the highest resolution available in the confocal stack. A parallel thinning algorithm was then applied to iteratively reduce the GFP-positive voxels in the three-dimensional biliary volume until a contiguous unit-width, medial axis "skeleton" was generated. Adapted from an existing algorithm (Wang & Basu, 2007), 62 templates were applied in parallel (multi-threading across multiple processors) to "delete" voxels that matched a given template's 26- or 124-neighbor configuration. Following this thinning process, Djikstra's shortest path algorithm was employed to thin any existing "crowded" regions to generate a final unit-width skeleton. Using similar voxel connectivity criteria, nodes (skeletal points with more than two voxels within its 26-neighbors), endpoints (skeletal points with only one voxel within its 26-neighbors), node-node skeletal segments, and node-endpoint skeletal segments were delineated. Each segment and node was given a unique identifier to enable visualization and path/distance tracking ("walk" from any segment or node to another segment or node) within the 3D network. Lastly, a Euclidean distance map was created using the original biliary volume and "multiplied" by the skeletal network to enable thickness characterization of any component within the network. We will make the Liver Analysis Program 5.3 software available upon request.

Supplementary Table 1

Western blotting and immunohistochemistry

Antibodies

Primary Antibody	Concentration	Assay	Company
Anti-Pak1	1:1000	WB	Abcam, Cambridge, MA, Cat. ab138710
anti-phospho-Pak1/2/3	1:1000	WB	Sigma, St. Louis, MO, Cat. P7746
anti-phospho-Pak1/2/3	1:200	IHC	Sigma, St. Louis, MO, Cat. P7746
anti-CLF1	1:1000	WB	Lifespan Biosciences, Seattle, WA, Cat. 358939
anti-phospho-Cofilin 1 (hSer3)	1:1000	WB	Santa Cruz Biotechnology, Dallas, TX, Cat. sc-12912-R C6
anti-ABCB11 rabbit polyclonal antibody	1:200	IHC	Kamiya biomedical, Tukwila, WA, Cat. MC-333
anti-PKC (C-20) rabbit IgG	1:200	IHC	Santa Cruz Biotechnology, Cat. SC-216
anti-Phospho-Histone H3	1:200	IHC	Cell Signaling Technology, Danvers, MA, Cat. 9701
anti-Cytokeratin 18 (Ks 18.4) monoclonal antibody	1:50	IHC	ProSci, Poway, CA, Cat. 49-082
anti-Anxa4 (2F11) monoclonal antibody	1:200	IHC	Abcam, Cat. Ab71286
anti-Beta-tubulin	1:5000	WB	Abcam, Cat. 6046

The following reagents were used for fluorescent staining: DAPI 1:200 (Sigma, Cat. D9542; 5ug/mL) and Alexa Fluor 647 Phalloidin 1:10 (Invitrogen, Waltham, MA, Cat. A22287).